THE OHIO STATE UNIVERSITY

IR and FIR Laser Diagnostics for Plasma Thrusters Using a CW CO_2 Radiation Source

Thomas M. York
Department of Aeronautical and Astronautical Engineering

Air Force Office of Scientific Research
Directorate of Aerospace Sciences
Bolling AFB, D.C. 20332

Grant No. AFOSR-89-0297
Final Report

July 1990

Unclassified
SECURITY CLASSIFICATION OF THIS PAGE

REPORT DOCUMENTATION PAGE

1a. REPORT SECURITY CLASSIFICATION Unclassified	1b. RESTRICTIVE MARKINGS
2a. SECURITY CLASSIFICATION AUTHORITY	3. DISTRIBUTION / AVAILABILITY OF REPORT Approved for public release Distribution unlimited
2b. DECLASSIFICATION / DOWNGRADING SCHEDULE	
4. PERFORMING ORGANIZATION REPORT NUMBER(S)	5. MONITORING ORGANIZATION REPORT NUMBER(S) AFOSR-TR-90-1030
6a. NAME OF PERFORMING ORGANIZATION The Ohio State University 6b. OFFICE SYMBOL (If applicable)	7a. NAME OF MONITORING ORGANIZATION AFOSR
6c. ADDRESS (City, State, and ZIP Code) 1314 Kinnear Road Columbus, OH 43212-1194	7b. ADDRESS (City, State, and ZIP Code) AFOSR/NA Bldg 410 Bolling AFB DC 20332-6448
8a. NAME OF FUNDING / SPONSORING ORGANIZATION AFOSR 8b. OFFICE SYMBOL (If applicable) NA	9. PROCUREMENT INSTRUMENT IDENTIFICATION NUMBER AFOSR-89-0297
8c. ADDRESS (City, State, and ZIP Code) AFOSR/NA Bldg 410 Bolling AFB DC 20332-6448	10. SOURCE OF FUNDING NUMBERS PROGRAM ELEMENT NO. 61102F; PROJECT NO. 2308; TASK NO. A1; WORK UNIT ACCESSION NO.
11. TITLE (Include Security Classification) "IR and FIR Laser Diagnostics for Plasma Thrusters Using a CW CO_2 Radiation Source" (U)	
12. PERSONAL AUTHOR(S) Dr Thomas M. York	
13a. TYPE OF REPORT FINAL 13b. TIME COVERED FROM 890501 TO 900430	14. DATE OF REPORT (Year, Month, Day) July 1990 15. PAGE COUNT 37
16. SUPPLEMENTARY NOTATION	

17. COSATI CODES			18. SUBJECT TERMS (Continue on reverse if necessary and identify by block number)
FIELD	GROUP	SUB-GROUP	
			Diagnostics, Plasma, Thruster

19. ABSTRACT (Continue on reverse if necessary and identify by block number)

The accomplishments during this contract period have been related to the development of a multi-beam interferometer system, which would utilize a CO_2 laser system for high sensitivity, to eventually be used to diagnose plasma in the electromagnetic expansion region of a plasma thruster. Since the application of interest is a 1/4 Scale MPD experiment, funded by NASA, where plasma is poorly known, the CO_2 laser interferometer will first be tested with a single beam on a DC discharge experiment whose plasma characteristics are well known. That experiment has been assembled and tested. The CO_2 laser system has been tested and found to be satisfactory.

20. DISTRIBUTION / AVAILABILITY OF ABSTRACT ☒ UNCLASSIFIED/UNLIMITED ☒ SAME AS RPT. ☒ DTIC USERS	21. ABSTRACT SECURITY CLASSIFICATION UNCLASSIFIED
22a. NAME OF RESPONSIBLE INDIVIDUAL Dr Mitat A. Birkan	22b. TELEPHONE (Include Area Code) (202) 767-4938 22c. OFFICE SYMBOL NA

DD FORM 1473, 84 MAR 83 APR edition may be used until exhausted. All other editions are obsolete.

SECURITY CLASSIFICATION OF THIS PAGE
UNCLASSIFIED

THE OHIO STATE UNIVERSITY

IR and FIR Laser Diagnostics for Plasma Thrusters Using a CW CO_2 Radiation Source

Thomas M. York
Department of Aeronautical and Astronautical Engineering

Air Force Office of Scientific Research
Directorate of Aerospace Sciences
Bolling AFB, D.C. 20332

Grant No. AFOSR-89-0297
Final Report
RF Project 767344/721902

July 1990

CONTENTS

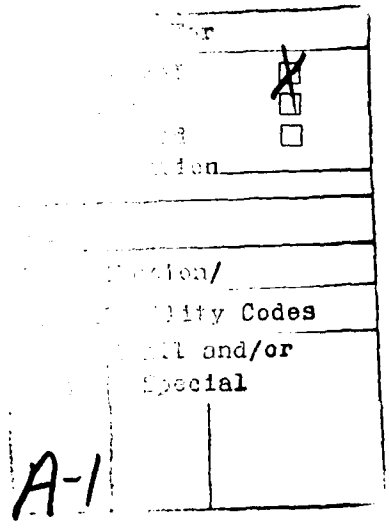

SUMMARY

The accomplishments during this contract period have been related to the development of a multi-beam interferometer system, which would utilize a CO_2 laser system for high sensitivity, to eventually be used to diagnose plasma in the electromagnetic expansion region of a plasma thruster. The laser system and supporting components were procured under an AFOSR (DoD) Instrumentation grant which ended 30 November 1989. Accordingly, the initial period of activity (May through Nov.) involved completion of detailed design considerations of the diagnostic system, negotiation of procurement agreements with vendors, assembly and testing of components as they were delivered. This process is continuing, since delivery of components has been continuous: only the detector electronic remain to be delivered. Further, numerous components were also designed and fabricated at the AARL. Since the application of interest is a 1/4 Scale MPD experiment, funded by NASA, where plasma is poorly known, the CO_2 laser interferometer will first be tested with a single beam on a DC discharge experiment whose plasma characteristics are well known. That experiment has been assembled and tested. The CO_2 laser system has been tested and found to be satisfactory. In the near future (1 month) the diagnostics will demonstrate proof-of-principle. Basic studies for examination of electron density fluctuations with the CO_2 laser have been initiated.

STATEMENT OF WORK
(As Proposed)

This effort will be directed toward the development and implementation of CO_2 laser based diagnostic systems for measurements on plasma thruster devices. The laser system is being procured under a DoD (AFOSR) Instrumentation Grant. This proposal requests support for operation so that the equipment can be developed and used on existing thruster experiments with other supporting and correlative diagnostics.

Research during the one-year period of requested funding will focus on the following activities:

1.) Design, development, and application of the CO_2 laser system with appropriate detectors to make multi-beam measurements of integrated line desity in thruster exhaust plasma. Reconstruction of Ne(r) as a function of time will be carried out at several axial locations in the exhaust.

2.) Evaluative studies of thruster plasma properties relative to implementation of Faraday rotation (Polarimetry) measurements of local magnetic (B) fields in the exhaust. This measurement must be made in the FIR (118 μm) and will depend on the interferometer measurements. Precise determination of sensitivity to the expected conditions as it relates to available optical components and detection will be made.

3.) Evaluative studies relative to fluctuation measurements in the thruster exhaust plasma will be carried out. The range of frequencies of fluctuations as they relate to available components and detectors are an important determination in the experiment design. The physics of this technique as it relates to anomalous transport will be an important determination.

RESEARCH ACCOMPLISHMENTS

1. Interferometry Diagnostic for Electron Density

One of the major parameters to be measured during a plasma discharge is the radially dependent electron density $N_e(r)$. Interferometry is used to measure quantities from which information can be extracted about $N_e(r)$.

When an electromagnetic wave propagates in a plasma discharge it undergoes a phase shift which is given by:

$$\phi = 2.82 \quad 10^{-13} \quad \lambda_o \int_{Z_1}^{Z_2} N_e(Z)\, dz$$

where ϕ = the phase shift

λ_o = the wavelength of the radiation

$N_e(z)$ = the chord dependent electron density

According to the formula above, the phase shift is proportional to the wavelength of the radiation used and the chord averaged electron density. Using simple interferometry ϕ can be measured, but the measurement is inaccurate due to the fact that the signal obtained is only proportional to the cosine of ϕ. Thus, it is impossible to determine if ϕ is increasing or decreasing. In addition to that, variations in the product of the scene beam with the reference beam can be incorrectly interpreted as due to changes in ϕ. To overcome these difficulties phase modulation should be used. That technique involves the following: the signal through one leg of the interferometer is first shifted up in frequency, then, as it propagates through the plasma it is phase modulated by an angle ϕ and eventually the frequency shifted, phase modulated signal is combined with the original source signal. The combined beam illuminates a detector and the detector output enters a comparator where it is compared to the modulation frequency. The comparator

outputs two signals, one is proportional to the cosine of the phase shift ϕ and the other is proportional to the sine of ϕ, thus, unambiguous calculation of the phase shift ϕ can be made. Knowing ϕ, the chord-averaged electron density, can be calculated. In order to calculate the radially dependent electron density a transformation must be applied on to the chord-averaged electron density. This transformation requires information about the chord-averaged electron density in several locations in the plasma and simple one channel interferometry is not able to provide that information. Thus, multi-beam interferometry vastly improves the cabability over one channel.

Since the phase shift, ϕ, is directly proportional to the wavelength of the radiation used, as shown in the formula above, longer wavelengths will produce larger ϕ values, thus making the phase shift easier to detect. During the first phase of this study, CO_2 laser radiation at 10.6 microns will be used for electron density measurements. FIR radiation (methyl alcohol laser at 118.9 microns) can be considered for the same electron density measurements.

1.1 Interferometry - Experiment

To date, the entire multi-beam interferometry experiment has been designed, and the indicated components of the hardware involved have been ordered. Components and their physical description are included in Appendix 1.

The optical scheme of the proposed multi-beam interferometer is shown in Figure 1. The experiment was initially designed with 5 independent channels but due to limited funds it will be assembled with only 4 channels. Should funding become available in the future, the 5th channel will be added.

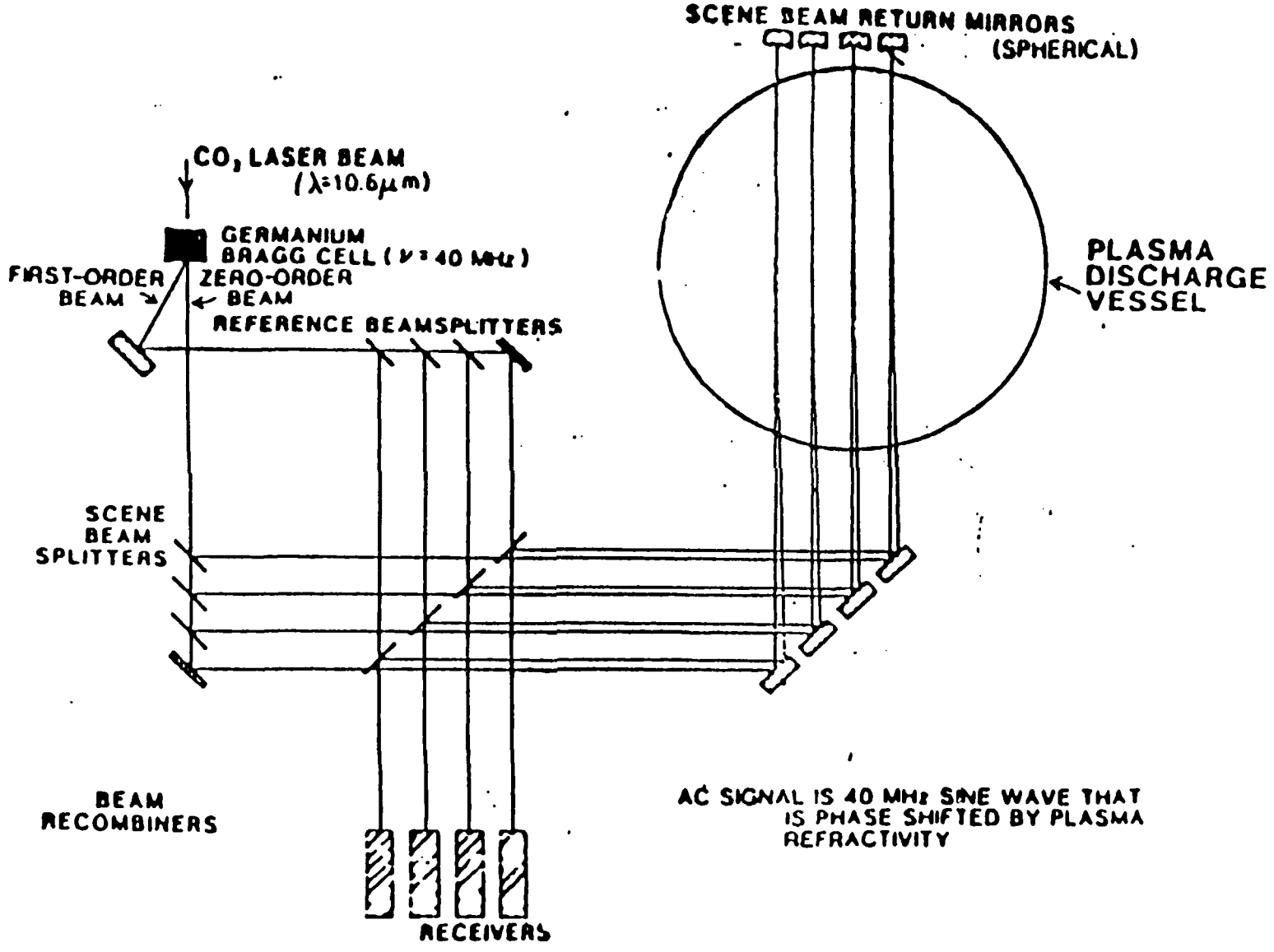

Figure 1: Schematic of Multi-Beam Interferometer

The output of the CO_2 laser (Apollo Laser Inc., Model 570) is down collimated from an 8mm diameter to a 5mm diameter and it then enters the germanium acousto-optic cell (Intra-Action Corp., Model AGM-406B). The acousto-optic modulator operates as a frequency shifter. It splits the input beam into two output beams, the scene beam (zero-order) and the reference beam (first-order), and shifts the frequency of the reference beam up by 40MHz with respect to the frequency of the scene beam. The first order beam illuminates the four reference paths of the interferometer and the zero order beam illuminates the four scene paths. The intensity of each one of the reference and scene beams is kept at about 20%. The paths of the scene beams proceed through the scene beamsplitters, to the reflecting flat mirrors, through the plasma to the reflecting concave mirrors, through the plasma for the second time to the flat mirrors again and finally onto the beam recombiners. The beam recombiners combine the reference beams as they come from the source with the scene beams as they come from the plasma; the combined output beams are focused onto the detectors.

The power detected contains an oscillating component at 40MHz due to the interference between the reference and the corresponding scene beams; it is also phase modulated due to the propagation of the scene beams through the plasma. All four receivers are the same. When the radiation is detected by the thermoelectrically cooled detectors (Electro-optical Systems Inc., Model MCT10-T1-002) a signal proportional to the input power is generated. The signal is amplified by a first stage amplifier and an amplifier and then enters the quadrature phase detector (Merrimac Industries Inc., Model PCM-3-40B). The phase detector generates two signals, one is proportional to the cosine of the phase shift due to the plasma and the other is proportional to the sine of the phase shift. The major advantage of this technique is that the phase shift can now be calculated unambiguously. A function generator set at 40MHz drives

each one of the four quadrature phase detectors and the acousto-optic cell. An eight channel waveform recorder (Gould Electronics, Model 4386) will be used to digitize and store all the sine and cosine signals while the experiment is in progress. The stored data will then be transferred through a IEEE-488 bus (Metrabyte, Model IE-488) to a PC (DELL Computer Corp., System 316SX) for further analysis. The commercially available scientific software ASYST 3.0 will be used for analysis and graphing/presentation purposes.

1.2 Preliminary Investigation of the Beam "Quality"

Before using the CO_2 laser system for the proposed experiment some external beam parameters will be measured. It is important that these parameters are known before the radiation is used for the diagnostic experiment because the obtained results will depend on them. The parameters that will be measured are as follows.

1.2.1 Intensity Profile of the Beam, Beam Size

The beam intensity pattern versus the distance across the beam (intensity profile) is of great importance. The intensity profile will be measured in both X and Y directions as shown in Figure 2, for both the near field portion of the beam and the far field portion of it. Knowing the intensity profile of the beam allows the determination of the beam size. The beam size is defined as the diameter of the beam that contains a usable percentage of the total beam energy. This diameter can be defined between positions where the intensity has fallen to the user selected, $1/e$, $1/e^2$, FWHM values with respect to the beam's peak intensity level. Figure 3 depicts that information.

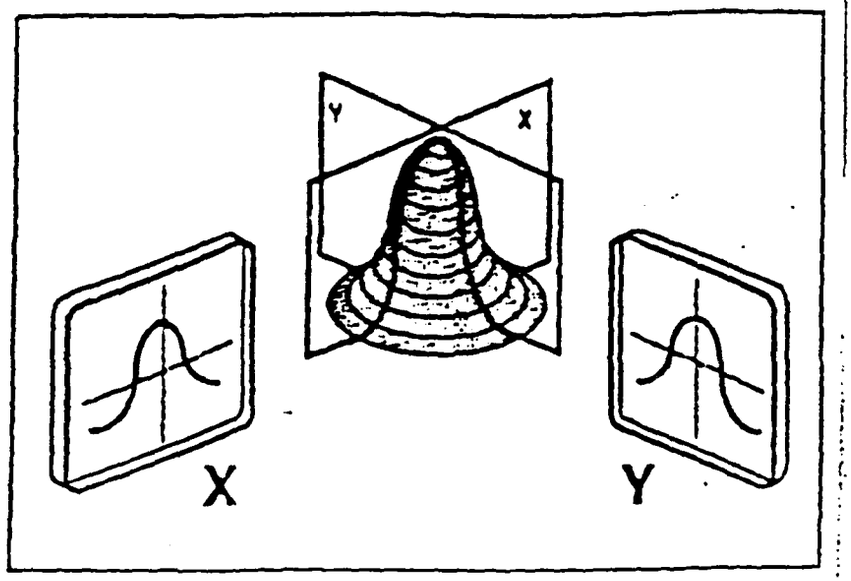

Figure 2: Intensity Measurements Made in X and Y Planes

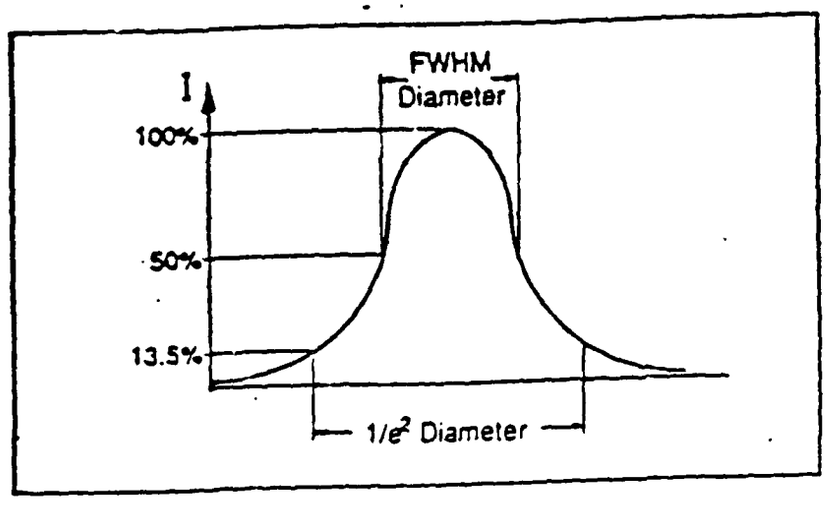

Figure 3: Definition of Beam Intensity Parameters

The intensity profile will be measured by scanning a detector sensitive to CO_2 radiation wavelength (10.6 microns) across the beam diameter and recording the power incident on the detector. The detector will be set on a motorized stage which will move across the beam with a predetermined constant speed. The detected power will be digitized and stored in the waveform recorder mentioned above for further analysis and plotting. In order to measure the intensity profile in the perpendicular direction, the motorized stage with the detector will be mounted in a 90 degree angle with respect to the latter position. Displaying the intensity profile on a monitor will determine whether the intensity distribution is the appropriate or not.

1.2.2 Beam Divergence

Another quantity which is desirable to know is the degree of collimation of the beam. Most beams change in size as they propagate, and the rate at which the beam grows is known as the divergence. This angular measure of the beam can be determined by knowing the intensity profile. First, two beam diameters, d1 and d2, will be measured at two different locations in the beam path, l1 and l2, respectively. Then the difference between the measured beam diameters divided by the distance between the points of measure will give the divergence angle. Implementing the above statement in an equation results in:

$$\text{Divergence angle} = \frac{d2 - d1}{l2 - l1}$$

The requirement that $l1 > (d^2/\text{wavelength})$ has also to be satisfied when the divergence is measured as stated above. Figure 4 is a sketch of the situation.

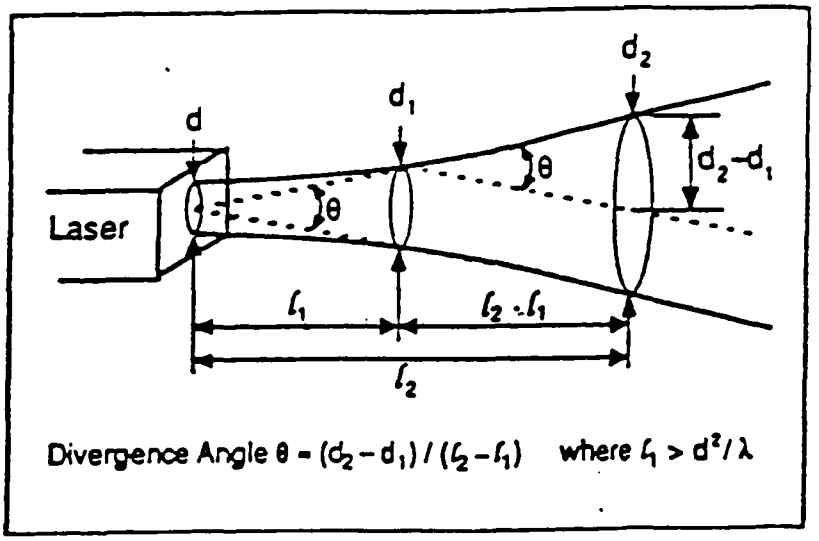

Figure 4: Determination of Beam Divergence Parameters

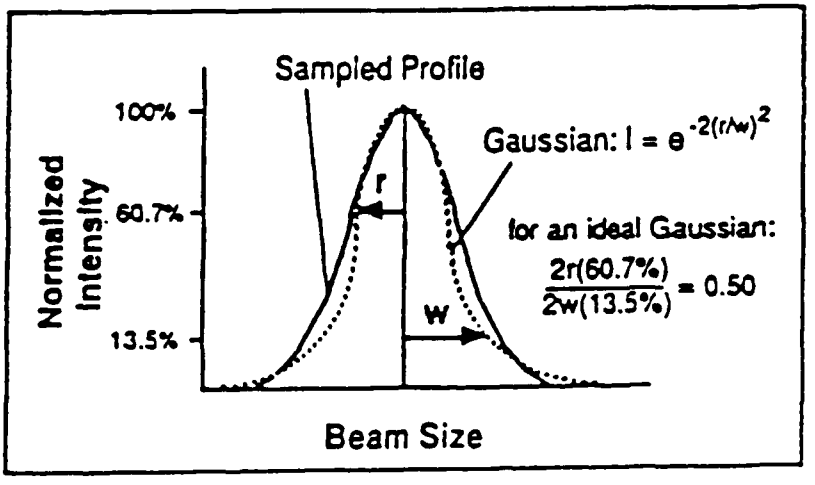

Figure 5: Identification of Beam Radiation Patterns

1.2.3 Laser Stability

Stability is a characteristic of both the frequency at which the that a laser operates and the output that it produces. For Apollo Laser Model 570, frequency stability is immediately achieved after tuning to a wavelength. On the other hand, the output power delivered by the laser is not stable for the first 2 meters of the beam path (ref. manufacturer). In order to clarify the behavior characteristic, the average power delivered will be measured with a power meter for a relatively long period of time; the data taken will be digitized and stored. The analysis of the data will involve calculations of the mean power, percent change in power, and standard deviation for all the samples taken ; the stability of the laser will be defined from the results.

1.2.4 Percentage Gaussian Beam in the Output Beam

The radiation pattern of a laser is closely linked to the characteristics of the laser resonator. Transverse modes refer to the patterns of light across the beam as they emerge directly from the laser. Apollo Model 570 will be operated in the TEM_{oo} mode. A TEM_{oo} mode has a smooth Gaussian profile while other higher order modes tend to cause the beam to spread. The percentage of Gaussian beam within a mixed mode beam can be determined by comparing the diameters at two intensity levels as shown in Figure 5.

2. Single-Beam Diagnostic Verification Using Test-Bed Discharge

The multi-beam interferometry experiment will involve four beams, applied to the 1/4-scale thruster experiment;, initial work underway involves only one beam. Assembly of a four beam interferometer for the first time without previous experience on tasks such as running the CO_2 laser, aligning the optics, working with the signal processing electronics (detectors, amplifiers, phase detectors, e.t.c.) was concluded to be unnecessarily difficult. Further, the 1/4 Scale MPD thruster is occupied at this time with a Thomson Scattering experiment and a Langmuir probe measurement set up, both of which have higher priority. Consequently, a more feasible approach involves the use of a well known set up a small plasma discharge to generate a test plasma and use the interferometric assembly described earlier to measure the electron density in the test plasma. Working with a one beam interferometer poses less difficulty and valuable experience will be gained which can be later applied to the four beam system.

2.1 Reference Plasma Generated by Test-Bed Discharge

The arc discharge circuit and its lumped equivalent model are presented in Figure 6 (Ref. 1). Although the circuit is simple, the presence of a time varying resistance, R(t), made analysis difficult. The R(t) term includes the arc itself where the resistance is a function of the discharge current. The difficulty of analysis exists since the exact relationship between the arc current and its resistance is not known. Thus, an exact, closed-form solution of the discharge current as a function time is not possible. The discharge current waveform is shown in Figure 7. It was found that the current reached a peak value of approximately 3200 A between 20-25 μs after the discharge began and the discharge current remained above 2500 A for a period of 20 μs. The electrical element values for the circuit are given in Figure 6. A 19.3 μF

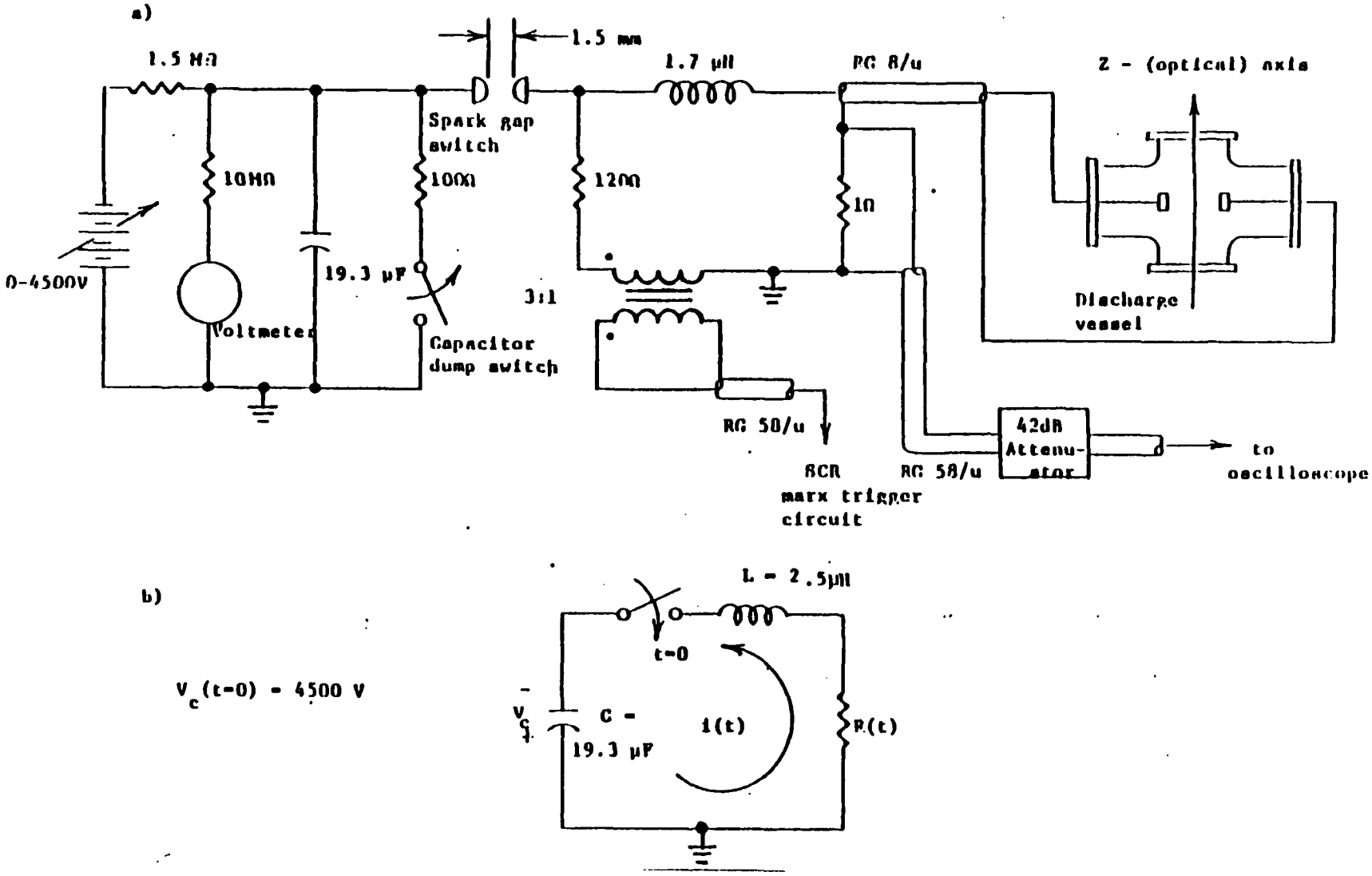

Figure 6: a) Reference Plasma Discharge Schematic, b) Equivalent Circuit after Spark Gap Switch has been Triggered

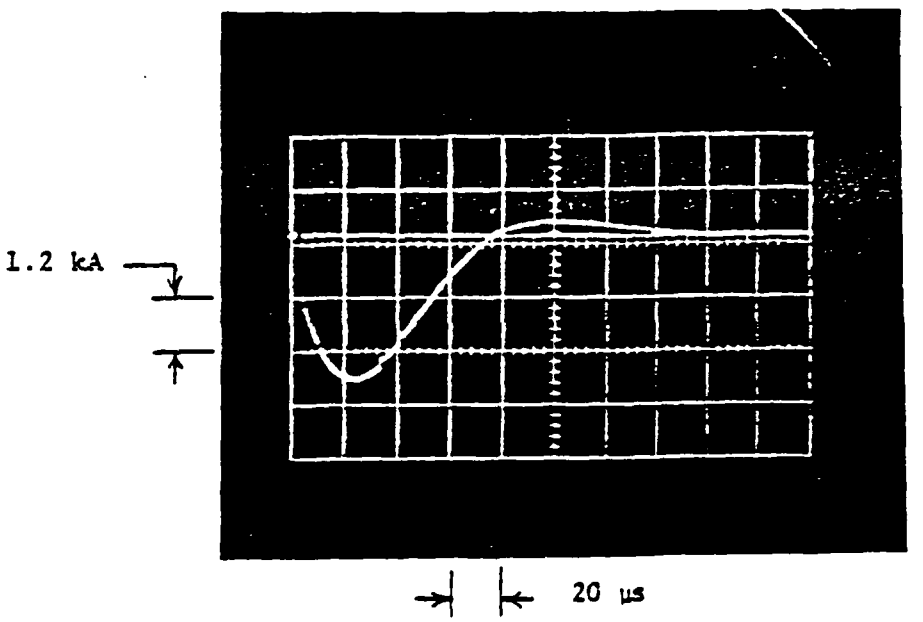

Figure 7: Plasma Discharge Current Waveform

capacitor was charged to -4500 V. The total circuit inductance was measured to be 2.5 μH, which agreed with a calculated value of 2.2 μH. A 1 Ω power resistor was added to the circuit to moderate the arc current. The voltage drop which developed across the resistor as a result of the arc current was input to a voltage divider network as shown in Figure 6. The voltage out of the voltage divider was proportional to the arc current and thus provided a monitor of the current. The fill gas within the discharge vessel was 50 mT air. The arc electrodes were 3.2 cm diamet aluminum discs separated by a distance of 5 cm, as shown in Figure 8.

The discharge was triggered when a + 7.5 kV pulse was delivered to the spark gap from the trigger circuitry. The capacitor was charged to -4500 V. The gap was set at 1.5 mm and held off voltages to -5 kV. When the positive pulse appeared across the gap, it broke down, thus providing a current path for the discharge. The circuit was slightly underdamped as shown in Figure 7, with current reversal at approximately 70 μs.

2.2 Double Langmuir Probe Reference Diagnostic

The reference diagnostic for evaluating the electron number density in the arc was a double Langmuir probe. This type of diagnostic has been shown to be accurate in indicating electron density in this range of plasma density (2).

The probe was integrated into an 8 mm O.D. pyrex tubing support which carried all wiring through a vacuum seal into the discharge vessel. The probe coaxial wiring was shielded up to the probe tip to reduce noise pickup. The probe tips were 0.006 inch (0.0152 cm) diameter tungsten wire, with a length of approximately 0.9 cm exposed to the plasma. The probe tips were aligned parallel with a spacing of 0.5 cm between them. The tungsten wire was encased in pyrex capillary tubing from the probe mount to the exposed portion of the tip.

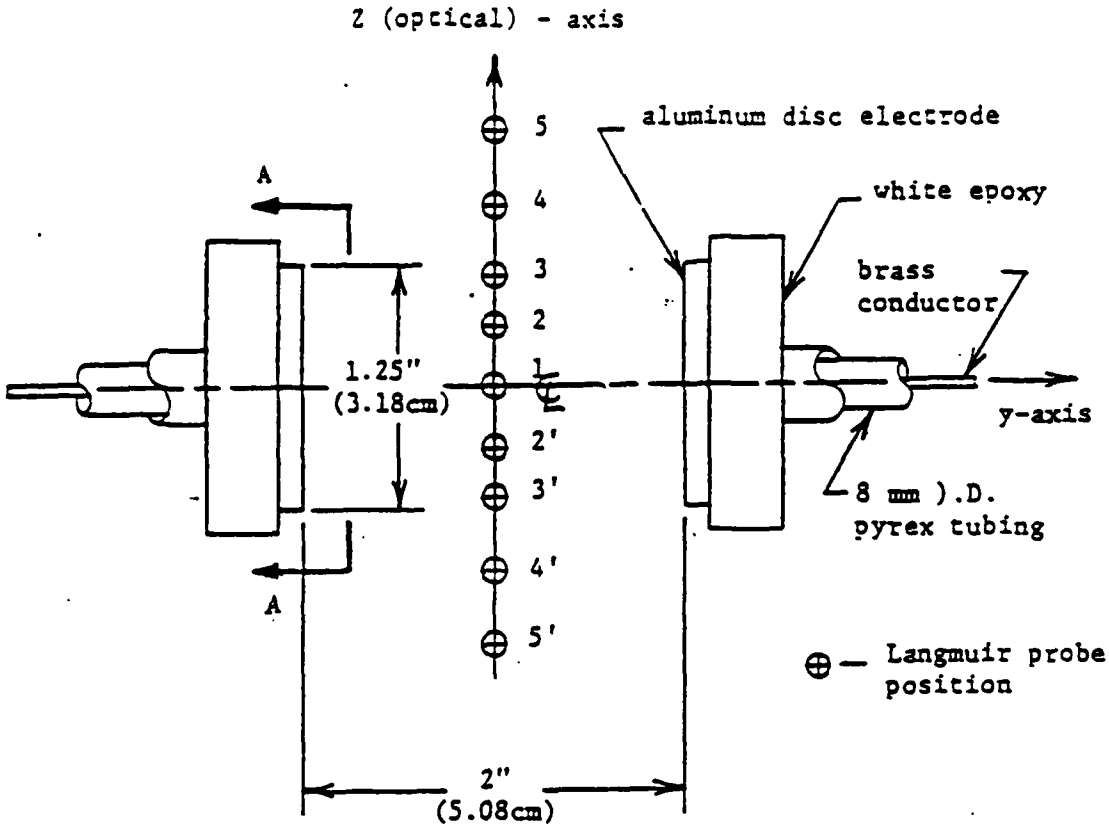

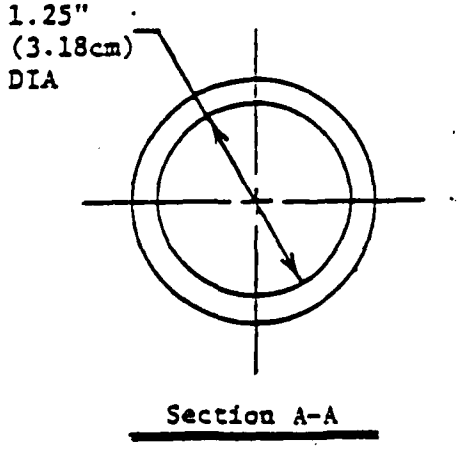

Position along the Z-axis	Distance from ℄ (y-axis, cm)
5	3.59
4	2.59
3	1.59
2	0.79
1	0.00
2'	-0.79
3'	-1.59
4'	-2.59
5'	-3.59

Figure 8: Discharge Electrodes and Respective Probe Positions Along the Z (optical) - Axis

2.3. The Fabry-Perot Interferometer Plasma Diagnostic

The electron number density data gathered on the arc discharge using the Langmuir probe has been compared with line density information provided by a Fabry-Perot Interferometer (FPI). That interferometer diagnostic is described briefly here. Line density measurements made with the FPI interferometer are compared with Langmuir probe results.

2.3.1 Experimental Device

The FPI experimental device can be divided into three components: The input side, the test cavity, and the output side. The experimental set-up is shown in Figure 9. The experiment was mounted on two aluminum channels, four feet (121.9 cm) long by one foot (30.5 cm) wide, positioned end to end. The channels themselves were supported by three columns of ten inch (25.4 cm) cement blocks with three blocks per column. Each column rested on a vibration isolation unit consisting of two pieces of slate sandwiching an automobile tire innertube. The isolation system attenuated mechanical vibrations from the floor and was extremely important in increasing the stability of the interferometer. The isolation helped to reduce noise in plasma measurements made with interferometer.

2.3.2 Comparison of Experimental Electron Line Density Results

The Langmuir probe data was used in conjunction with a zeroth order Bessel function in order to model the electron density distribution and thereby calculate the line density. The electron line density was obtained by integrating the density distribution along the optical axis. On the other hand, the FPI yielded electron line density directly. The line density was found by multiplying the average electron density by the distance over which the probing beam travels through the plasma. Line density data versus time obtained for the arc discharge are presented in Figure 10.

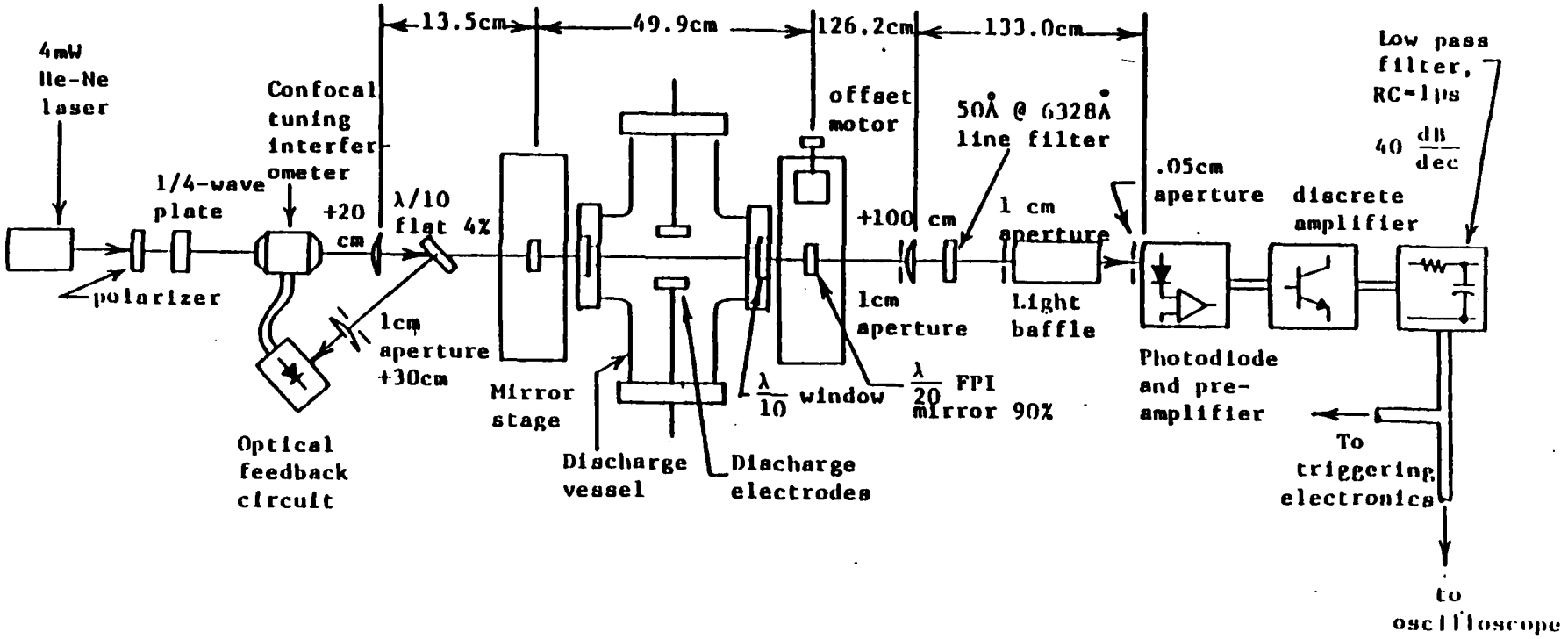

Figure 9: Fabry-Perot Interferometer Experimental Lay-Out

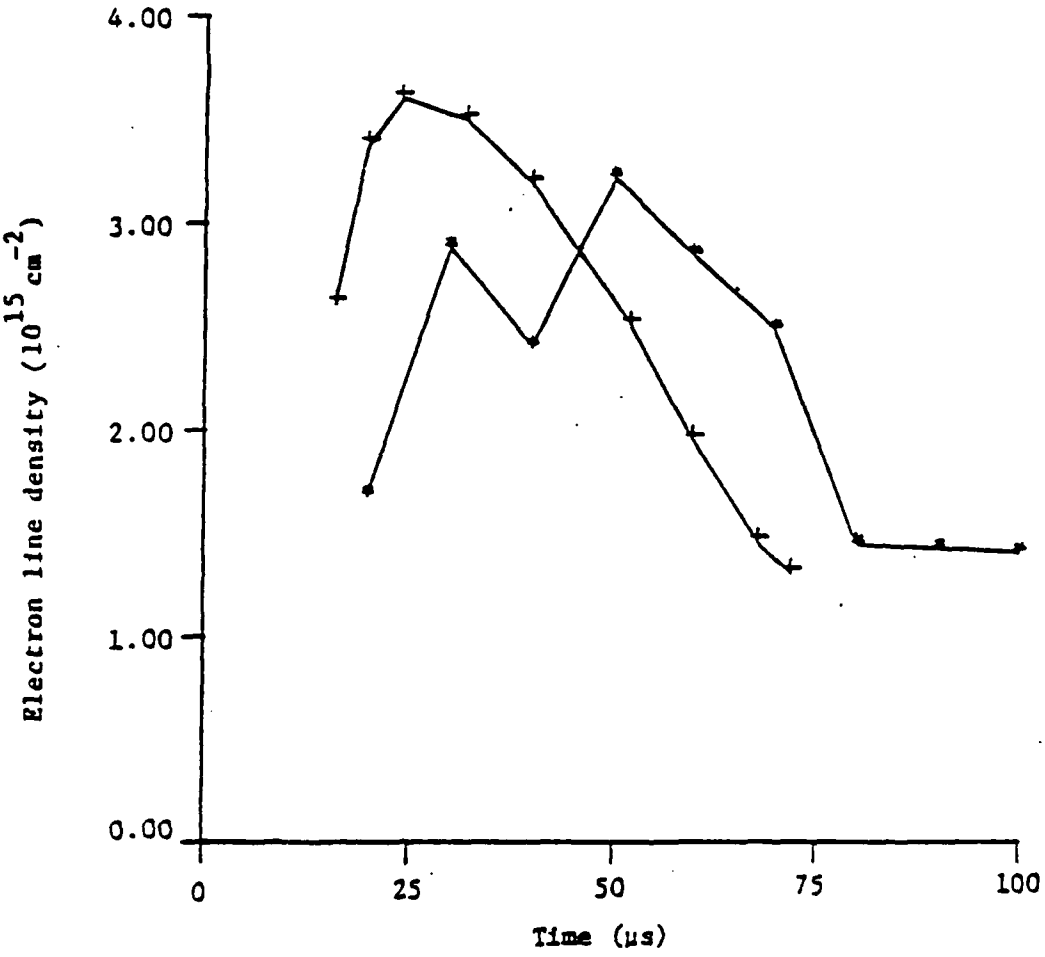

Figure 10: Electron Line Density Versus Time from Both Langmuir Probe (+) and FPI (*) Data

Comparison of the two variations of electron line density versus time in Figure 10 shows that overall, the Fabry-Perot interferometer and the Langmuir probe plasma diagnostics are in good agreement with one another. Both diagnostics indicate a maximum electron line density of approximately $3x10^{15}$ cm^{-2}. However, several specific differences in the two results may also be observed.

Most notably, the line density calculated using the probe data reached a maximum approximately 25 μs after the initiation of the discharge; whereas the interferometer indicated the maximum to occur later, about 50 μs after the beginning of the arc.

The differences in the electron line density results may have occurred for several reasons. First, though the two diagnostics are used to calculate the same quantity, the line density, they in fact measure two things. The probe measures electron number density at a specific point; whereas, the interferometer views the entire electron population along its optical path thereby integrating to obtain a density per cross sectional area of beam or line density. Therefore, the interferometer loses the distribution information which is provided by a number density diagnostic such as the Langmuir probe.

It is likely that 10 to 20 μs must elapse before an equilibrium distribution can be established; the reason for this time lag is important. Since the Langmuir probe was positioned close to the center of the arc for most measurements, it is reasonable to assume that line density derived from this data would be different from that calculated using the interferometer. The interferometer views the entire distribution of free electrons, not just their density at one point as does the Langmuir probe. Probe data taken from records at different positions with respect to the electrode centerline shows, in fact, that the probe current reaches a maximum later in time at positions further from the arc.

3. Experimental Studies of 1/4-Scale MPD Thruster Acceleration

(NASA Lewis Supported)

In order to operate the ¼-scale MPD thruster and to successfully employ simple diagnostics, alterations to the thruster itself and to the test facility had to be made from that designed for the AFAL facility. The most important change to the experimental apparatus was in the development of a gas feed system for the thruster. This effort included the fabrication of a pulse generating circuit to operate a Skinner Solenoidal valve (Model V520B2100, Honeywell Skinner Valve Division, New Bruton, CT) that controlled the gas feed to the thruster. The test facility electrical circuits were altered in order to obtain reliable measurements that were free of external noise. These changes were made after a comprehensive evaluation of the grounding and shielding systems was performed. Also included in the changes to the test facility was the addition of a switching system which allows the thruster bank and the magnetic field bank to be charged to different voltage levels. Voltage on both banks could be monitored.

3.1 Gas Feed System for the Thruster

The gas feed system for the ¼-scale MPD thruster was designed, within available resources, to reliably provide a uniform gas flow into the thruster electrical discharge chamber. The transient time before achieving a steady-state flow was made as short as possible in order to minimize the back pressure build up in the vacuum chamber. The major components of the gas feed system are shown in Figure 11. They include the thruster plenum, the reserve plenum, and the Skinner valve connecting the two plenums.

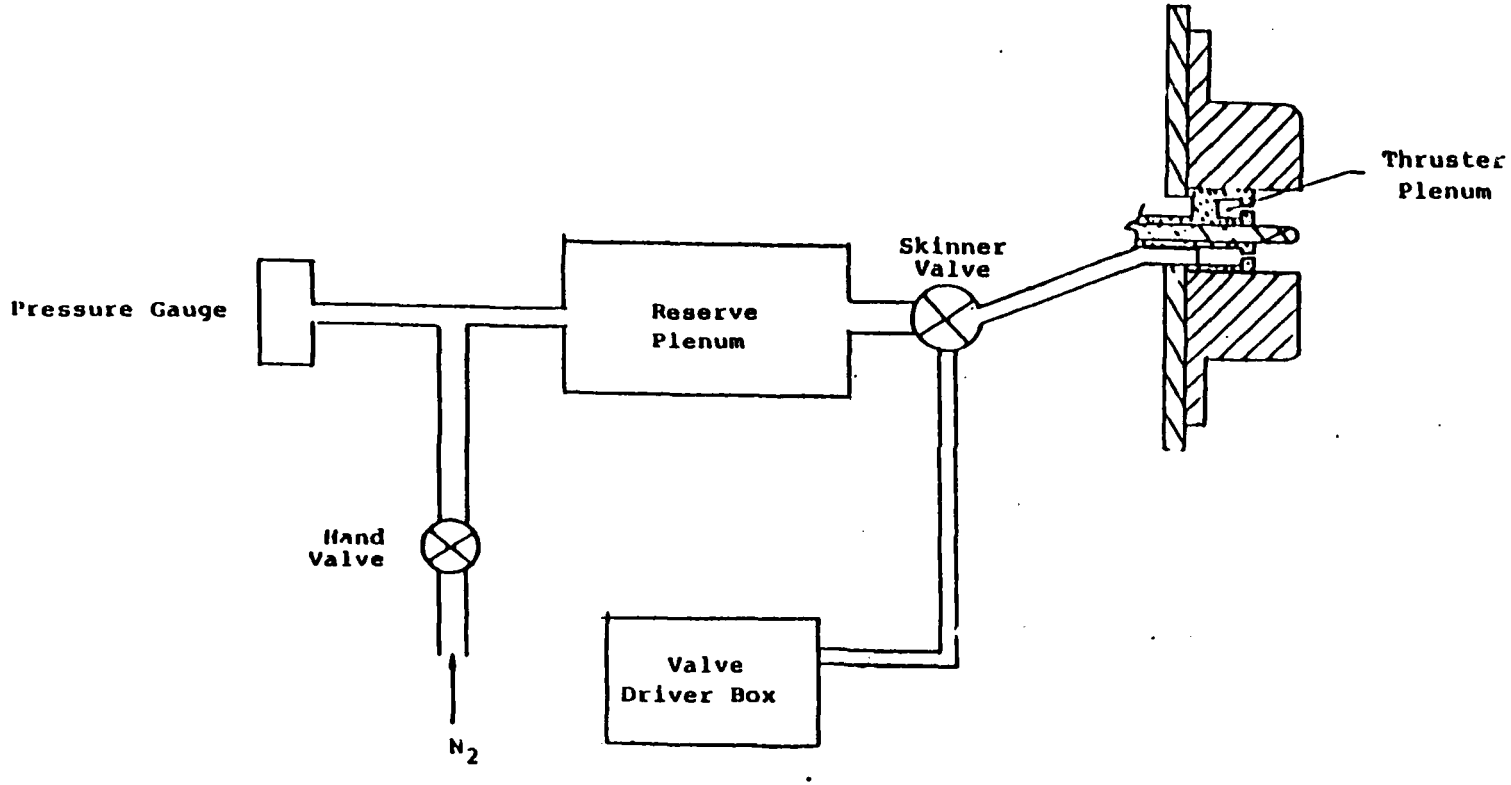

Figure 11: Gas Feed System Components

The back pressure in the vacuum chamber was estimated with the known behavior of the mass flow rate and the volume of the vacuum chamber. The mass flow rate at which the thruster was operated for all of the data presented in this report was 0.135 gm/sec. This mass flow rate was chosen for reasons to be discussed in the following section. This mass flow rate corresponds to an estimated back pressure of 7 mTorr at the time of firing. These parameters are listed in Table 1 with comparisons between the ¼-scale thruster and those reported from full-scale devices. The numbers shown for the Princeton full-scale thruster have been calculated from the information given in Reference (3). While back pressure effects on thruster performance have been widely reported, some studies have indicated that this level of back pressure may have only slight effects on the self-field performance.[4]

Table 1: Comparison of Operating Condition for 1/4-Scale and Full-Scale MPD Thrusters

	Initial Pressure (torr)	Scaled $\dot{m}$ (gm/sec)	Pressure at Ignition (torr)	Pressure at End of Discharge (torr)
1/4-Scale	$> 1x10^{-3}$	0.135	$7.0x10^{-3}$	$7.7x10^{-3}$
Full-Scale (Princeton)	$> 1x10^{-5}$	2.16	$3.24x10^{-3}$	$4.1x10^{-3}$

3.3 Operation and Characteristics of the ¼-Scale MPD

The operating characteristics of the ¼-scale MPD were first examined by measuring the electrical characteristics. These electrical characteristics include the current-voltage trends across the anode and cathode, and the distribution of current in the exhaust plume. Results from initial current-voltage measurements led to an increase over ideal scaled values of the mass flow rate for thruster operation. Results from local magnetic field probes used

to map the enclosed current in the exhaust plume, led to a change in the thruster mass injection scheme. Both of these changes improved the operating characteristics of the thruster and produced a stable arc. Current-voltage behavior with and without magnetic fields shown in Figure 12.

3.4 Thruster Diagnostic Studies: Magnetic Field and Impact Pressure

The two primary diagnostics used to examine the exhaust field of the ¼-scale MPD thruster were magnetic field probes and piezoelectric pressure probes. The magnetic field probes were used to measure magnetic field strengths and enclosed currents within the exhaust plume Figure 13; the pressure probe was used to measure local impact pressures of the exhaust plume Figure 14. The information obtained from these probes was then used to examine the operation of the ¼-scale MPD.

These results clearly indicate that the applied magnetic field is compressing the plasma, forcing it to remain in a narrow radius, and allowing a more gradually expansion than a purely self-field case.

From the pressure profiles an indication of thrust and hence specific impulse can be obtained. Assuming the impact pressure is of the form $P_{impact}=(n_e+n_i)\,KT + n_i m_i V^2$, as previously done (5), integration of the impact pressure over the exhaust area will yield the thrust produced by the 1/4-scale MPD. Initial analysis shows that for the self field case thrusts of 1.2 N and 3.0 N for the 1.15 kA and 2.3 kA current levels, respectively, were achieved. For the applied field cases the thrust was increased to 1.9 N for 1.15 kA and to 5.1

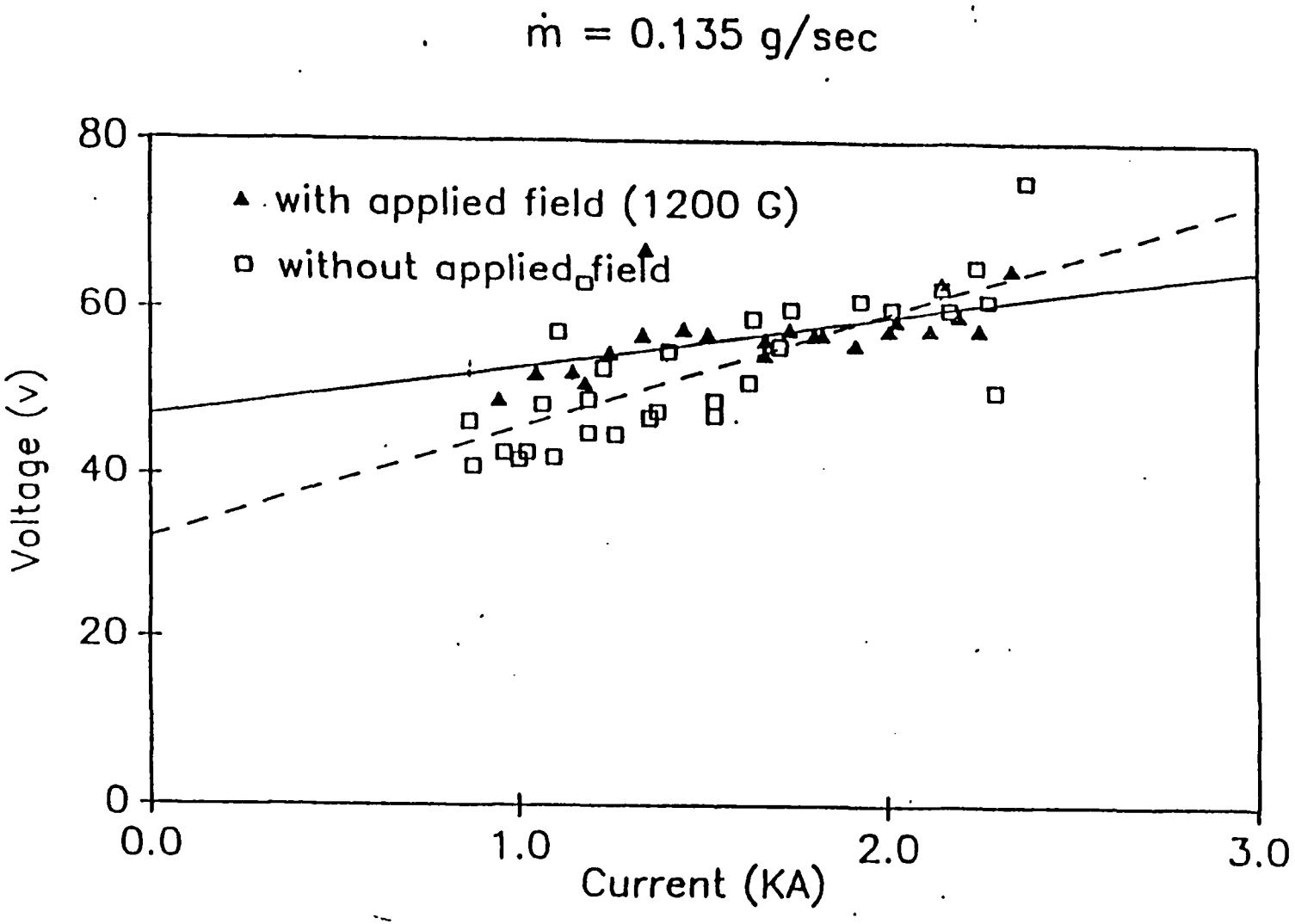

Figure 12: Current-Voltage Characteristics of the 1/4-Scale MPD

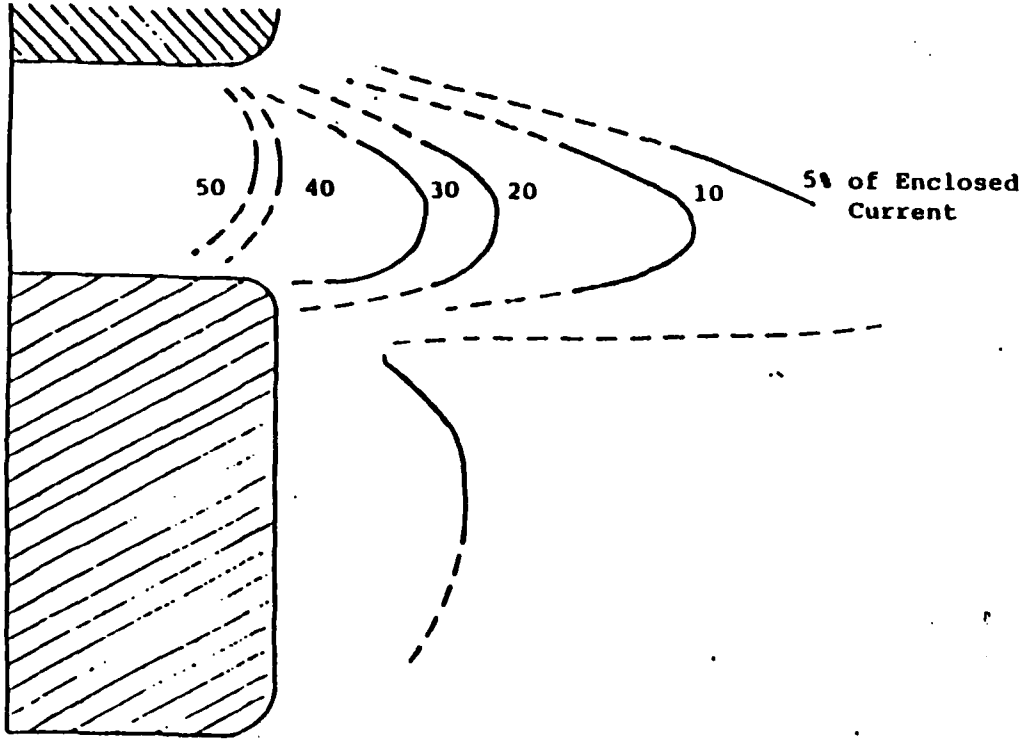

Figure 13a: Enclosed Current Profiles without Applied Magnetic Field (I=2.3kA)

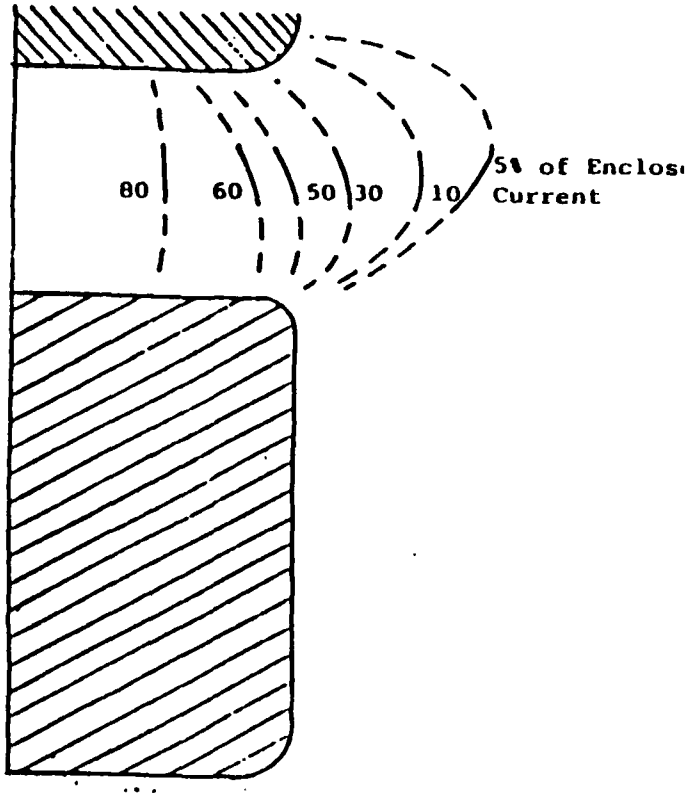

Figure 13b: Enclosed Current Profiles with Applied Magnetic Field (I=2.3kA)

Figure 13: Enclosed Current Profiles

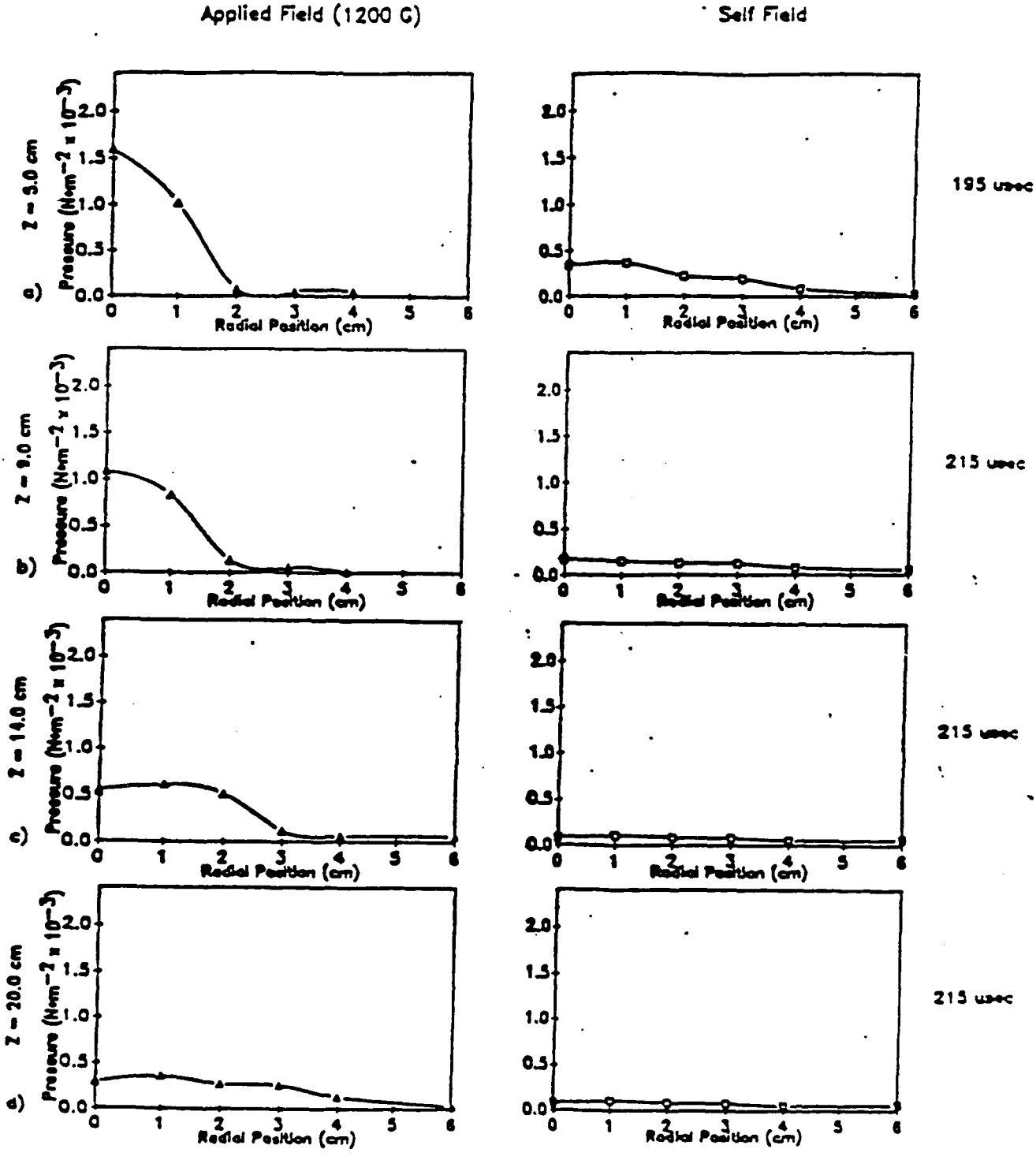

Figure 14a: Impact Pressure Profiles for I=1.15kA and m=0.135gm/sec

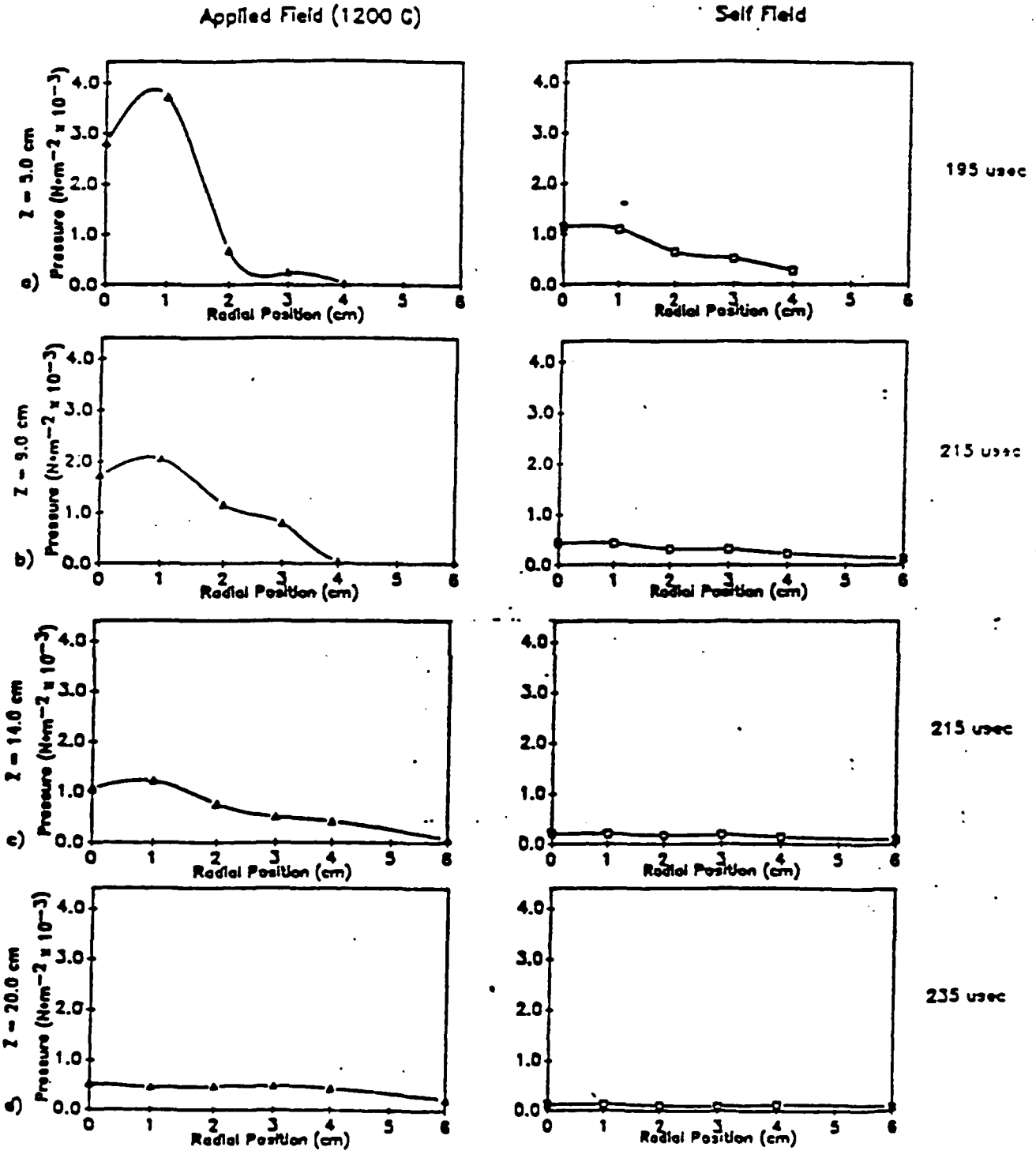

Figure 14b: Impact Pressure Profiles for I=2.3kA and m=0.135gm/sec

N for 2.3 kA. Using the relationship,

$$\bar{I}_{SP} = \frac{T}{\dot{m}g}$$

the specific impulse's for the various cases were determined. For the 1.15 kA level the self-field case has an I_{SP} of 880 sec while the applied field increases this to 1460 sec. For the 2.3 kA level the self case shows an I_{SP} of 2270 sec while the applied field increase this to 3830 sec. While a more detailed analysis of the thruster operation is needed to determine the physical process responsible for the effects of the applied magnetic field on the 1/4-scale MPD, these results clearly indicate that the applied magnetic field significantly improves the operation of the thruster by increasing thrust and thus specific impulse.

Faculty and Staff Participation
(By Funding)

T. M. York	Principal Investigator September 1989 - June 1990	5%
D. S. Emmer	Senior Researcher July 1989 - June 1990	10%
N. Kiritsis	Graduate Research Associate August 1989 - June 1990	50%

REFERENCES

1. Dooling, J. C., "The Evaluation of Electron Line Diagnostics on an Arc Discharge using a Fabry-Perot Interferometer," MS Thesis, Elec. Eng, The Penn State University, 1983.

2. Chung, P.M., Talbot, L., and Touryan, K. J., Electric Probes in Stationary and Flowing Plasmas, Theory and Application, Springer-Verlag, New York, 1975, p. 2.

3. Kaplan, D. J., "Performance Characteristics of Geometrically Scaled MPD Thrusters," M.S.E. Thesis, Princeton University, Princeton, NJ, February 1982.

4. Sovey, J.D. and Mantenieks, M. A., "Performance and Lifetime Assessment of MPD Arc Thruster Technology," AIAA Paper 88-3211, AIAA 24th Joint Propulsion Conference, Boston, MA, July 11-13, 1988.

5. Michels, C. J. and York, T. M., "Exhaust Flow and Propulsion Characteristics of Pulsed MPD Arc Thruster," AIAA Paper 72-500, April 1972.

Appendix

Appendix 1

Description of the Laser and Interferometer Equipment

1. Apollo Lasers Inc., Model 122

Model 122 is an optically pumped, submillimeter resonator. The system consists of a tunable CO_2 laser (Model 570) and a FIR resonator fully integrated. Model 570 which serves as the optical pump for the submillimeter resonator is tunable to more than 85 wavelengths in the 9.17 to 10.91 micron range. It features excellent stability in output amplitude and frequency and can be operated CW, chopped or pulsed. The output power in the TEM mode ranges from a minimum of 30 watts to 55 watts on the strongest lines. A simple manually operated grating angle adjustment allows the user to select anyone of more than 85 wavelengths and frequency stability is immediate. In the pulsed mode, the Model 570 can deliver power five times the CW power at the same wavelength.

The submillimeter waveguide resonator is a variable length Fabry-Perot resonator. It includes the appropriate hole-coupled reflectors to allow oscillation over a wide range of far infrared wavelengths.

The output of the Model 570 is folded by means of two reflectors and focused within the FIR resonator. A polar molecular gas in the resonator (C2H50H, methyl alcohol), at low pressure is excited by the incident CO_2 energy and undergoes a rotational transition emitting energy in the far infrared. The resonator is a 1.5 meter long dielectric waveguide whose output reflector can be manually translated to adjust cavity length, optimizing the FIR output power. The system also includes a feedback loop to stabilize the power in the FIR laser. The Model LCS-1 corrects the CO_2 cavity length in response to drifts in FIR power.

Model 122 has been delivered and it is ready for the initial checkout. The CO_2 gas tank (6% Carbon Dioxide, 18% Nitrogen and 84% Helium) is connected to the laser and its cooling system is ready to operate.

2. Neslab, Model RTE-110B CO_2 Laser Cooling System

Model RTE-100B is a constant temperature bath operating between -30 degrees C and +100 degrees C. The desired bath temperate is set on the temperature controller and the bath is kept at that level + or - 0.1 degree C. The system is equipped with a circulating pump which circulate the water through the device to be cooled. Model RTE-101B is connected to the cooling system circuitry of the CO_2 laser head. Water is circulating around the head constantly at the rate of 0.5 gal/min to remove the excess head generated.

3. Intra-Action Inc., Acousto-Optic Cell with its Driver

The AGM-406B acousto-optic cell utilizes Bragg deflection of light by an acoustic beam. When RF voltage is applied to the piezoelectric transducers, acoustic waves are generated in the solid interaction medium. Associated with this acoustic wave is a strain induced change of refraction index of the solid medium. an incident light beam will be defracted as it passes through the region occupied by the travelling acoustic wave. If the incident light beam strikes the acoustic wave fronts at a proper angle, the Bragg angle, efficient deflection of the light beam occurs. At 10.6 micron wavelength the Bragg angle

is approximately equal to 2.21 degrees. The defracted beam is also upshifted in frequency by an amount equal to the RF carrier frequency. This experiment requires the RF signal that drives the acousto-optic cell to be synchronous with the signal that drives the quadrature phase detectors. Thus the driver of the cell (AGM-408C) has been modified to accept an external driving RF signal. For the purpose of this experiment the externally applied modulation frequency is 40MDz. Models AGM-406B and AGM-408C have been ordered from Intra-Action Corp. and were shipped on the 16th of January 1990.

4. Optics for Research, Mirrors, Beamsplitters, Lenses

All the optical components ordered are 1 inch in diameter and 1/8th of an inch in thickness. Two kinds of mirrors were ordered, flat and concave. The flat mirrors (7 pieces) are designed for 45 degrees incidence and the concave mirrors (4 pieces) have 2 meters of curvature. Both types of mirrors have a reflectance of about 99%+. The beamsplitters are made out of zinc zelenide material in order to be transparent to 10.6 micron radiation, they are AR coated on one surface, S-polarized and are designed for 45 degrees incidence. Their specified reflectivities/tranmisivities as they go down the two legs of the interferometer are: 20/80 (2 pieces), 25/75 (2 pieces, 33/67 (2 pieces) and 50/50 (6 pieces). The reference beamsplitters on the figure are 50/50 beamsplitters. The reflectivities/tranmisivities are designed as such in order for the reflected beam to be always 20% of the initial beam power. The lenses are also made out of zinc zelenide material, they are AR coated on both surfaces and have a positive focal length of 80 millimeters.

5. Electro-Optical Systems Inc., Detectors/Amplifiers

The MCT10-T1-002 detector is a high performance photoconductive HgCdTe (mercury cadmium tellurite) device designed specifically to detect CO_2 radiation (10.6 microns). The unit includes the detector element, typically 20 to 50 ohms resistance, a two-stage thermoelectric cooler with a thermistor type temperature sensor, a sealed package/heat sink with germanium window AR coated for 10.6 microns, and optionally an amplifier and signal conditioning electronics. The system has the capability of greater than 100 MHz bandwidths and NEP values of a few nanowatts/Hz 1/2. The cooler operates down to -45 degrees C (no load) with less than 2 watts of input power.

The photoconductive element requires a fixed bias current of approximately 50mA. As the 10.6 micron radiation strikes the element, the resistance drops, creating a voltage drop across the element which is then amplified and conditioned as the system requires. The detector noise levels are in the range of nanovolts/Hz 1/2 so care must be taken in the design of the amplifier and bias circuits to insure proper performance.

6. Merrimac Ind. Inc., PCM-3-40B Quadrature Phase Detectors

Merrimac's Quadrature Phase Detectors provide two output voltages which together permit unambiguous phase comparisons to be made over the entire 0 to 360 degree phase shift range. The detectors compare the unknown phase shifted signal coming from the CO_2 radiation detectors to the reference 40MHz signal coming from the function generator and outputs two signals. One is proportional to the sine of the phase difference between the reference and the unknown input signals and the other is proportional to the cosine of this phase

difference. The PCM-3-40B are custom made quadrature phase detectors centered at 40MHz with a 10% bandwidth.

7. Wavetek, Model 166 50 MHz Pulse/Function Generator

The Model 166 combines the features of a function generator, a sweep generator, and a pulse generator into one package. The function generator supplies both normal and inverted sine, triangle, and square waves over the frequency range of 0.0001Hz to 50 MHz. The waveforms can be continuous, triggered, double triggered and gated. The sweep generator varies the main generator's output up to full 1000: 1 limit of each frequency range. The pulse generator procedures pulses with independent variable transition times and widths. These pulses can be continuous, triggered, double triggered and gated as well as swept. Its output range goes up to 30 V peak-to-peak or 15 V peak-to-peak into a 15 Ohm resistor. This relatively high output is needed in order to drive the 5 quadrature phase detectors and the acousto-optic cell. Since model 166 has only one output channel but is required to drive 6 other devices simultaneously, six emitter follower circuits have to be built to split that one output channel of 40 MHz frequency into six.

8. Gould Electronics, Model 4386 Waveform Recorder

Model 4386 is a high frequency multi-channel waveform recorder. It is equipped with eight single ended channels each one having its own 8-bit A/D converter. The input measurement range varies from 50mV to 500V full scale in 13 calibrated input ranges with variable gain. There are 10 selectable sample rates from 500 samples/second to 1/3 Megasamples/second. Due to the high sampling rate, Model 4386 features 32K/channel on board memory (32,768 words per channel). The data are stored on its own memory after they are sampled and digitized. All channels are sampled simultaneously to avoid time skew between channels. Flexible triggering allows to precisely capture the waveform or transient, with up to 100% pretrigger data, for cause-effect analysis. Store data can be transferred repeatably for analog plotting at various speeds or in digital form at high speed via the IEEE-488 standard interface.

9. DELL Computer Corp, System 316SX

The DELL system 316SX delivers 386/16MHz performance and runs advanced 32-bit software designed for Intel 80386-based microprocessors. The unit purchased comes with 1MB or RAM memory, 40MB-29ms hard disk drive, less than one wait state, color VGA screen with a resolution of 480 x 600 pixels and 16-bit video adapter, an Intel 16MHz 80387 math co-processor, one 5.25" high density (1.2MB) and one 3.5" high density (1.44MB) floppy diskette drives, 1 parallel and 2 serial ports, 6 (full-size) 16-bit and 2 (1 full-size, 1 half-size) 8-bit expansion slots, enhanced 101-keyboard, 200-watt power supply and MS DOS Version 3.3 operating system. The CPU is housed in a bigger box with dimensions: width=21.1", height=6.4", depth=17.6", which allows the insertion of electronic boards depending on the future needs.

10. Metrabyte, IE-488 Interface Bus

The GPIB/IEEE-488 bus is the communication port between the waveform

recorder and the PC> IT is a 16-bit card which is placed in one of the PC's expansion slots. The acquired data will be transferred from the waveform recorder's storage memory to the computer through this bus. The bus is controllable from the ASYST 3.0 software described below.

11. Keithley, ASYST 3.0 Scientific Software

ASYST 3.0 is an integrated software system designed for scientific and engineering applications. ASYST 3.0 offers sophisticated analysis, graphics, data acquisition and instrument control via Analog-to-Digital, Digital-to-Analog and RS-232 and GPIB/IEEE-488 instrument interfaces. All the ASYST capabilities are accessed and/or modified through English-based commands. ASYST 3.0 is fully integrated, allowing the user to switch smoothly between acquiring, analyzing and viewing the data. ASYST 3.0 is comprised of four modules; Modules 1, 2, 3, and 4. Only Modules 1, 2 and 4 were purchased because Module 3 is the data acquisition and control module and for that purpose the waveform recorder Model 4386 by Gould Electronics will be used. Modules 1 and 2 is the basic ASYST 3.0 software. This software is capable of doing the following: a) Basic math (complete arithmetic operations, including all trigonometric functions, exponatiation and logarithms), b) can handle single and double precession, integer, real and complex data type numbers, c (it interfaces to Microsoft C (version 5) and Fortran (version 4.1), d) its waveform processing capabilities include: waveform arithmetic, Fast Fourier Transform (FFT), Inverse FFT, 2D-FFT, I2D-FFT, smoothing, clipping, convolution, filtering, peak detection, integration, differentiation, e) its curve fitting capabilities include: goodness-of-fit reporting, correlation matrices, cross correlation, weighted and non-weighted fits, etc., f) it can handle polynomial and matrix math (matrix inversion, determinants, diagonalization, polynomial shifting, root extraction, etc., g) it can handle statistics (basic statistical functions, gaussian distributions, sort, sort and index, random number generation, histograms, etc., h) it can do graphics X-Y plots, auto-scaling and data fitting, contour plots, log, linear and polar plots, error bars, etc. Module 4 includes the control software for the GPIB-IEEE-488 bus. ASYST 3.0 with its documentation has already been delivered and installed in the computer.

3.12 Optical Engineering Inc., Model CO_2 Spectrum Analyzer

The CO_2 spectrum analyzer is a grating spectroscope which simultaneously displays all the lasing transactions of a CO_2 laser. It is calibrated both in wavelength and rotational line designation to permit easy identification of 140 possible laser transitions between 9.1 and 11.3 microns. These transitions are visually displayed through the use of a UV excited thermal sensitive screen which darkens in the area struck by the IR laser beam. All the transition lines are displayed simultaneously giving an accurate representation of the complete spectrum.

13. Optical Engineering Inc., Model CO_2 Laser Power Probe

Due to the fact that in most laboratory situations a quick check of the power is required with minimum disruption, a laser probe was purchased. The probe is a self contained unit consisting of an absorbing head, a temperature measuring mechanism, a zeroing knob and a readout dial. The probe is exposed

to the laser beam for a specified time interval and after the power probe has been removed from the laser beam the average laser power can be read out on the dial. The power probe purchased has a power range up to 50 Watts, exposure time of 20 seconds and it can be used to measure power in laser beams with maximum diameter of 1 inch. The absorbing head is only about 0.5 inches thick which makes it easy to be inserted between instruments close together.

14. Optical Engineering Inc., CO_2 Laser Probes

The CO_2 laser beam probes are hand-held plates designed to simplify the alignment of IR optical systems. They display the laser beam as a dark image on a florescent background using UV excited, thermal-sensitive surfaces. Their small size permits them to be placed close to optical parts and accurately show the position of the laser beam relative to an aperture. Two such probes were purchased with different power ranges. One probe responds to powers between 100-30 W/cm2 and the other to powers between 25-7.5 W/cm2.

15. Apollo Laser Inc., Model 101 CO_2 Laser Power Meter

The Model 101 laser power meter consists of a direct absorption convection water cooled head mounted on a table top stand and a small electronics assembly with a digital readout meter. It is designed to measure radiated laser power in the CW mode over the wavelength range of 0.3 to 30 microns. The sensor head can dissipate up to 200 watts continuously if it is water cooled or up to 100 Watts without water cooling. When incident radiation strikes the center of the non reflective sensing disk, heat is conducted rapidly outward its periphery. A thermopile mounted on the back of the disk, senses a radial temperature differential and as a result a voltage is generated. The thermopile output voltage is amplified, conditioned and scaled so a direct readout in Watts appears on the LCD display.

16. Scientech, Model 36-0001 FIR Power Meter

There was an extensive market search for a power meter that could operate in the 119 micron wavelength range (C2H5OH laser wavelength) but not such meter could be found. Instead, reference number 3 was found where Scientech's Model 36-0001 power meter with range of 0.25 to 35 microns was tested for radiations longer than 35 microns (up to 5000 microns). The test produced a calibration factor of 0.8 when the meter was used with 118.9 micron radiation (methyl-alcohol laser). Based on the fact that Model 36-0001 had been calibrated by others for the methyl-alcohol laser wavelength and also that the recommended readout unit to be used with it was already available in the lab, the decision to use it as the FIR power meter was taken.

Model 36-0001 is a surface absorbing disc calorimeter. Incident radiation is absorbed by the special coating which is applied on the head and eventually a voltage proportional to the incident power is generated. Model 365 is a microprocessor controlled laser power-energy meter which reads the information supplied by Model 36-0001, converts it into Watts/Joules and displays it on an LCD screen. It also features both digital and analog outputs. The analog output gives 0.1 V full scale. The digital output is a standard serial output (RS232). The serial output transmits ASCII data at a baud rate determined by an internal program. This allows the meter to be used in computerized data

collection. Since it responds to 1Q.6 micron wavelength, Model 36-0001 will be used for the power stability measurements of the CO_2 laser.

1132.tmy/rd